Research Journal of Recent Sciences _____ ISSN 2277-2502
Vol. **1(8),** 1-9, August **(2012)** *Res.J.Recent Sci.*

Numerical Analysis of Direct Injection Diesel Engine Combustion using Extended Coherent Flame 3-Zone Model

Renganathan Manimaran[1], Rajagopal Thundil Karuppa Raj[2] and Senthil Kumar K.[3]
[1,3]Thermal and Automotive Division, School of Mechanical and Building Sciences, VIT University, Vellore, INDIA
[2]Energy Division, School of Mechanical and Building Sciences, VIT University, Vellore, INDIA

Available online at: www.isca.in
Received 15th March 2012, revised 26th March 2012, accepted 28th March 2012

Abstract

Several applications have proven the reliability of using multi-dimensional CFD tools to assist in diesel engine research, design and development. CFD tools are extensively used to reveal details about invisible in-cylinder processes of diesel combustion so that guidance can be provided to improve engine designs in terms of emissions reduction and fuel economy. Innovative combustion concepts can be evaluated numerically prior to experimental tests to reduce the number of investigated parameters. In this present work, reacting flow simulations were performed in a single cylinder direct injection diesel engine with an improved version of the ECFM-3Z (extended coherent flame model – 3 Zones) model using ES-ICE and STAR-CD codes. Combustion and emission characteristics are studied in a sector of engine cylinder, which eliminates the tedious experimental task with conservation in resources and time. The pressure variations during motoring and firing conditions, temperature and heat release graphs with respect to crank angle are plotted. Mass fractions contours of CO, NO, soot and fuel ($C_{12}H_{26}$) and mixture density contours at TDC are plotted. It is found that higher NOx emissions occur at peak temperatures while soot and CO emissions occur at peak pressures.

Keywords: Direct injection, ECFM-3Z model, combustion, emissions.

Introduction

Compression Ignition (CI) diesel engines are employed for heavy-duty usage as they can develop more power at lesser fuel consumption. Different methods of fuel supply are used for CI engines, namely indirect and direct type. Out of these different types of engines, the direct-injection (DI) diesel engine exhibits the best fuel economy along with lowest emissions. The best fuel economy in a vehicle is developed with the modern DI diesel engine. This trend is facilitated by the development of contemporary injection systems that are more flexible, and generate higher injection pressures for better spray atomization and combustion characteristics than their predecessors. The modern DI diesel engines satisfy stringent emission norms without after treatment.

The complex task of improving internal combustion engines, which have reached a higher degree of sophistication, can be achieved by the combination of advanced experiments and computational studies. The quantitative uncertainties of numerical simulations are often greater than those of experiments[1]. The modeling of combustion engine processes has significant advantages in understanding the heat release rate and formation of reactant species.

Recent efforts to reduce pollutant emissions and fuel consumption have resulted in the development of many advanced combustion concepts. Among them, low temperature combustion is attracting more interest since it has been proven in many studies that the exhaust gas recirculation helps the combustion processes avoid from NOx and soot formation environments[2,3]. In practical applications, premixed charge compression ignition (PCCI) realizes low temperature combustion by injecting fuel very early (- 40 deg ATDC) to produce a premixed fuel air charge prior to the ignition[4,5]. In PCCI combustion, the flash boiling occurs easily because of the early fuel injection into the cylinder which is low pressure and temperature because in-cylinder pressure and temperature decrease with advancing of the fuel injection. Another methodology namely modulated kinetics (MK)[6] requires late injection with a large amount of cooled recycled exhaust gases to delay ignition timing and thus lower the combustion temperature. However, these approaches usually result in higher unburnt hydrocarbons (UHC) and CO emissions compared to conventional diesel engine combustion. To achieve low-temperature combustion in a diesel engine, a highly dilute environment is usually required, namely, low in-homogeneity of the in-cylinder charge with a large EGR rate even up to 60%. The energy efficiency improvement can be achieved by improving the design and technology by suitable turbocharging techniques[7]. CO2 emission reduction potential through three strategies in technological improvement which are installation of blended winglets, installation of dryers, and installation of air units are considered[8].

The ECFM (Extended Coherent Flame Model) is a version of the flame surface density approach, which allows the simulation of the diffusion and premixed combustion modes as well as

knock and pollutant formation, even in highly stratified cases. Based on this model, the unified diesel combustion model ECFM-3Z was briefly explained in the literature[9]. In order to account for diffusion flame and mixing processes, each computational cell is split into three mixing zones: a pure fuel zone, a pure air and residual gases (EGR) zone and a mixed zone. This structure allows to account for the three main combustion modes encountered in most combustion devices.

The aim of this paper is to simulate the combustion in diesel engine using ECFM-3Z model in detail. Combustion and emission characteristics of the fuel n-Dodecane are studied here. The importance of this work is to exhibit the capability of numerical modeling the combustion and emission characteristics rather than experimental work and to understand the physics underlying the direct injection diesel engine combustion.

Mathematical Models: The three dimensional in-cylinder, transient, non-reacting flow physics in a direct injection diesel engine is simulated by solving the following governing equations: i. Conservation of mass, ii. Conservation of momentum

The equations are provided in tensor notations[10].

$$\frac{\partial \rho}{\partial t}+\frac{\partial}{\partial x_j}(\rho u_j) = S_m \quad (1)$$

$$\frac{\partial}{\partial t}(\rho u_i)+\frac{\partial}{\partial x_j}(\rho u_j u_i - \tau_{ij}) = -\frac{\partial p}{\partial x_i}+S_i \quad (2)$$

where t – time and x_i – Cartesian coordinate (i=1,2,3), u_i – absolute fluid velocity component in direction x_i, p - static pressure, S_m and S_i are source terms for equations for conservation of mass and momentum respectively. The flow being assumed to be Newtonian, the following constitutive relation is specified connecting the components of the stress tensor τ_{ij} to the velocity gradients:

$$\tau_{ij} = 2\mu S_{ij} - \frac{2}{3}\mu \frac{\partial u_k}{\partial x_k}\delta_{ij} - \overline{\rho u_i` u_j`} \quad (3)$$

where μ - molecular fluid dynamic viscosity, δ_{ij} - kronecker delta =1(i=j) and 0 (otherwise), S_{ij} – rate of strain tensor $= \frac{1}{2}\left(\frac{\partial u_i}{\partial x_j}+\frac{\partial u_j}{\partial x_i}\right)$

The rightmost terms in equation (3) represents the additional Reynolds stresses due to turbulent motion and u` are the fluctuations about the ensemble average velocity. The Reynolds stresses are linked to the mean velocity fields via turbulence models using standard k-ε model as given.

Turbulence Modeling: The in-cylinder flow is turbulent in nature at all speeds and dimensions of the engine[11]. It is necessary to model the turbulence to capture the properties of in-cylinder fluid dynamics. The 'Standard' $k-\varepsilon$ model is which the turbulent Reynolds number forms of the k and ε equations are used in conjunction with the algebraic 'law of the wall' representation of flow, heat and mass transfer for the near wall region. All forms of the $k-\varepsilon$ models assume that the turbulent Reynolds stresses and the scalar fluxes are linked to the ensemble averaged flow properties in an analogous fashion to their laminar flow counterparts[12]:

$$\overline{\rho u_i` u_j`} = \mu_t S_{ij} - \frac{2}{3}\left(\mu_t \frac{\partial u_k}{\partial x_k}+\rho k\right)\delta_{ij} \quad (4)$$

$$\overline{\rho u_j` h`} = -\frac{\mu_t}{\sigma_{h,t}}\frac{\partial h}{\partial x_j} \quad (5)$$

$$\overline{\rho u_j` m_k`} = -\frac{\mu_t}{\sigma_{m,t}}\frac{\partial m_k}{\partial x_j} \quad (6)$$

$$k \equiv \frac{\overline{u_i` u_i`}}{2} \quad (7)$$

where k – turbulent kinetic energy, μ_t - turbulent viscosity, $\sigma_{h,t}$ - turbulent Prandtl number, $\sigma_{m,t}$ - turbulent Schmidt number, μ_t - turbulent viscosity = $f_\mu \frac{C_\mu \rho k^2}{\varepsilon}$, where C_μ is an empirical coefficient, usually taken as a constant and f_μ is the damping function, to be defined when the individual model variants are presented.

Standard $k-\varepsilon$ Model: The particular high Reynolds number form of the $k-\varepsilon$ model used is appropriate to fully turbulent, compressible or incompressible flows[13]. The transport equations are as follows:

Turbulent kinetic energy

$$\frac{\partial}{\partial t}(\rho k)+\frac{\partial}{\partial x_j}\left[\rho u_j k - \left(\mu+\frac{\mu^t}{\sigma_k}\right)\frac{\partial k}{\partial x_j}\right] = \mu_t (P+P_B)-\rho\varepsilon - \frac{2}{3}\left(\mu_t \frac{\partial u^i}{\partial x_i}+\rho k\right)\frac{\partial u^i}{\partial x_i}+\mu_t P_{NL} \quad (8)$$

where

$$P \equiv S_{ij}\frac{\partial u_i}{\partial x_j},\ P_B \equiv -\frac{g_i}{\sigma_{h,t}}\frac{1}{\rho}\frac{\partial \rho}{\partial x_i},\ P_{NL} = -\frac{\rho}{\mu_t}\overline{u_i` u_j`}\frac{\partial u_i}{\partial x_j} - \left[P - \frac{2}{3}\left(\frac{\partial u_i}{\partial x_i}+\frac{\rho k}{\mu_t}\right)\frac{\partial u_i}{\partial x_i}\right]$$

$P_{NL} = 0$ for linear models

Turbulent dissipation rate

$$\frac{\partial}{\partial t}(\rho\varepsilon)+\frac{\partial}{\partial x_j}\left(\rho u_j \varepsilon - \left(\mu+\frac{\mu_t}{\sigma_\varepsilon}\right)\frac{\partial \varepsilon}{\partial x_j}\right) = C_{\varepsilon 1}\frac{\varepsilon}{k}\left[\mu_t P - \frac{2}{3}\left(\mu_t \frac{\partial u_i}{\partial x_i}+\rho k\right)\frac{\partial u_i}{\partial x_i}\right] + C_{\varepsilon 3}\frac{\varepsilon}{k}\mu_t P_B - C_{\varepsilon 2}\rho\frac{\varepsilon^2}{k} + C_{\varepsilon 4}\rho\varepsilon\frac{\partial u_i}{\partial x_i} + C_{\varepsilon 1}\frac{\varepsilon}{k}\mu_t P_{NL} \quad (9)$$

Where $C_{\varepsilon 1}, C_{\varepsilon 2}, C_{\varepsilon 3}$ *and* $C_{\varepsilon 4}$ are coefficients whose values are given in table 1[14].

Conservation equations for heat transfer

$$\frac{\partial}{\partial t}(\rho h)+\frac{\partial}{\partial x_j}(\rho h u_j - F_{h,j}) = \frac{\partial P}{\partial t}+u_j\frac{\partial p}{\partial x_j}+\tau_{ij}\frac{\partial u_i}{\partial x_j}+S_h \quad (10)$$

Where 'h' is static enthalpy, defined by:

$$h \equiv \bar{c}_p T - c_p^0 T_0 + \sum m_k H_k = h_t + \sum m_k H_k \quad (11)$$

and T- temperature, m_k – mass fraction of mixture constituent k, H_k – heat of formation of constituent k, $\bar{c}_p$ – mean constant pressure specific heat at temperature T, $\bar{c}_p^0$ - reference specific heat temperature T_0, $F_{h,j}$ – diffusional energy flux in direction x_j = $k \frac{\partial T}{\partial x_j} - \bar{\rho}\,\overline{u_j' h'} + \sum_k h_k \rho D_k \frac{\partial m_k}{\partial x_j}$, where the middle term represents the turbulent flux of energy whose model is given later, S_h – energy source and h_t - thermal enthalpy. The static enthalpy, h is defined as the sum of the thermal and chemical components, the latter being included to cater for chemically reacting flows.

Conservation Equations for Species or Mass Transfer: Each constituent, k of a fluid mixture, whose local concentration is expressed as a mass fraction m_k, is assumed to be governed by a species conservation equation of the form:

$$\frac{\partial}{\partial t}(\rho m_k) + \frac{\partial}{\partial x_j}(\rho m_k u_j - F_{k,j}) = S_k \quad (12)$$

Where $F_{k,j}$ – diffusional flux component $= \rho D_k \frac{\partial m_k}{\partial x_j} - \bar{\rho}\,\overline{u_j' m_k'}$.

The rightmost term representing the turbulent mass flux whose model is given later, S_k – rate of mass production or consumption due to chemical reaction.

$$\sum_k m_k = 1 \quad (13)$$

Combustion and Ignition Models: The ECFM-3Z model[15] is a general purpose combustion model capable of simulating the complex mechanisms of turbulent mixing, flame propagation, diffusion combustion[16] and pollutant emission that characterize modern internal combustion engines. It can also be used for in-cylinder analysis in a multi-injection environment and for multi-cycle simulations. '3Z' stands for three zones of mixing, namely the unmixed fuel zone, the mixed gases zone, and unmixed air plus EGR zone. The three zones are too small to be resolved by the mesh and are therefore modeled as sub-grid quantities. The mixed zone is the result of turbulent and molecular mixing between gases in the other two zones and is where combustion takes place.

Droplet Breakup Models: Reitz and Diwakar model: Droplets from the nozzle enters the combustion chamber at high velocity and gets sheared at the outer periphery. Hence a model to disintegrate the droplets is given by Reitz and Diwakar model. Droplet break-up due to aerodynamic forces occurs in one of the following modes. i. 'Bag break-up', in which the non-uniform pressure field around the droplet causes it to expand in the low-pressure wake region and eventually disintegrate when surface tension forces are overcome. ii. 'Stripping break-up', a process in which liquid is sheared or stripped from the droplet surface.

In each case, theoretical studies have provided a criterion for the onset of break-up and concurrently an estimate of the stable droplet diameter, and the characteristic time scale of the break-up process[17,18].

Huh's Atomisation Model: Huh's model is based on the gas inertia and the internal turbulence stresses generated in the nozzle. A conceptual picture can be described in two stages: i. The turbulence generated in the nozzle hole produces initial perturbations on the jet surface when it exits the hole. ii. Once the perturbations have reached a certain level, they grow exponentially via pressure forces induced through interaction with the surrounding gas (surface wave growth), until these perturbations become detached from the jet surface as droplets. The model estimates the initial perturbations from an analysis of the flow through the hole and then uses established wave growth theory, coupled with other hypotheses, to represent the atomisation process.

Bai's Spray Impingement Model: This spray impingement model[19] is formulated within the framework of the lagrangian approach in order to reflect the stochastic nature of the impingement process, a random procedure is adopted to determine some of the droplet post-impingement quantities. This allows secondary droplets resulting from a primary droplet splash to have a distribution of sizes and velocities.

NOx Formation: Nitrogen oxides are important air pollutants, mainly produced by combustion devices. The NOx concentration is low in most of these devices; therefore, it has little influence on the flow field. Also, the time scale for NOx reactions is larger than the time scales for the turbulent mixing process and the combustion of hydrocarbons that control the heat-releasing reactions. Hence, computations of NOx can be decoupled from the main reacting flow field predictions. Three different mechanisms have been identified for the formation of nitric oxide during the combustion of hydrocarbons, namely:

Thermal NOx: As its name suggests, it is strongly temperature dependent. It is produced by the reaction of atmospheric nitrogen with oxygen at elevated temperatures[20].

Prompt NOx: The exact details of prompt NOx formation[21] are still uncertain but are generally believed to involve the reactions between hydrocarbon radicals and atmospheric nitrogen. In certain combustion environments (such as low temperature, fuel-rich conditions and short residence time), prompt NOx can be produced in significant quantities.

Fuel NOx: This is produced by the reaction of the nitrogenous components present in liquid or solid fossil fuel with oxygen[22]. The fuel nitrogen is a particularly important source of nitrogen oxide emissions for residual fuel oil and coal, which typically contain 0.3 - 2.0% nitrogen by weight.

Table-1
Coefficients of the Standard $k-\varepsilon$ turbulence model

C_μ	σ_k	σ_ε	σ_h	σ_m	$C_{\varepsilon 1}$	$C_{\varepsilon 2}$	$C_{\varepsilon 3}$	$C_{\varepsilon 4}$	K	E
0.09	1.0	1.22	0.9	0.9	1.44	1.92	0.0 or 1.44*	-0.33	0.419	9.0**

Soot Modelling: The formation and emission of carbonaceous particles is a process that is often observed during the combustion of hydrocarbons. These particulates, called soot, are identified in flames and fires as yellow luminescence. One class of modeling soot formation is based on specifying detailed reaction mechanisms for the gas phase chemistry and the formation, growth and oxidation of soot particles. The first approach, due to Mauss and his colleagues[23], is based on the laminar flamelet concept in which all scalar quantities are related to the mixture fraction and scalar dissipation rate. Whereas the species mass fractions are unique functions in the mixture fraction-scalar dissipation space, the soot mass fractions are not. The rates of soot formation can, however, be correlated with local conditions in diffusion flames or in partially premixed counterflow twin flames.

Table-2
Engine Specifications

Bore & Stroke	130 mm & 158 mm
Connecting Rod Length	270 mm
Compression Ratio	15.5
Engine Speed	1100 RPM
Crank Angle Start	680 deg
Crank Angle Stop	800 deg
Fuel	n-Dodecane
Fuel injection quantity	0.0367 kg
Start of Fuel Injection	6 deg bTDC
Fuel Injection Duration	8 deg

Material and Methods

The bowl geometry is chosen to be mexican hat and the bore and stroke details are given in table 2. Spline is obtained from the CAD model and trimming command is used to create a 30 degree sector. Radial, axial and piston top cells are selected appropriately and sector geometry is prepared as shown in figure 1. Initial and boundary conditions are set up in ES-ICE code and the computations are proceeded using STAR-CD code. The computations are performed in a Intel Xeon CPU (3.30 GHz, 3.24 GB RAM). The total elapsed CPU time is nearly 10 hours for a total of 4400 timesteps which leads to total time period of 18.2 milliseconds. Fuel injection starts as 714.75^o CA and stops at 722.25^o CA. Auto-ignition in the cells takes place at 719 ^{o} CA or nearly at 1200 timesteps. Grid independence test is carried out and found that cylinder sector with 16792 cells at TDC and 85236 cells at 800^o CA gives reproducible results. Simulation is performed with 60 radial cells, 16 azimuthal cells and 130 axial cells in a 30 degree sector of engine cylinder.

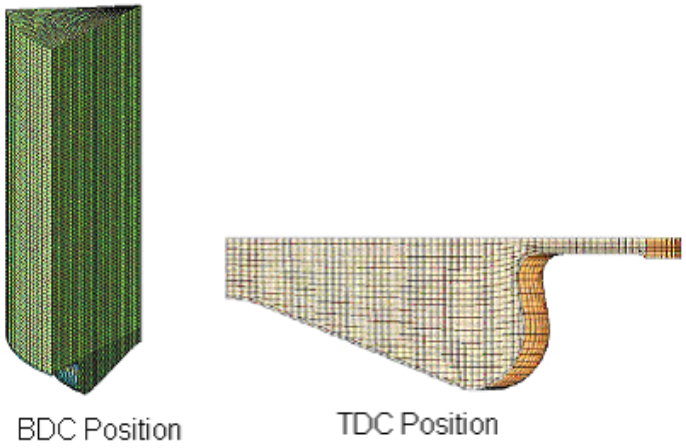

Figure-1
Computational domain of engine cylinder at TDC and BDC

Table-3
Initialization and Boundary conditions in DI Diesel engine sector

Cetane number	60
Swirl Ratio	1.81
Turbulence Intensity	10 %
Equivalence Ratio	0.85
Exhaust Gas Recirculation	10 %
Combustion dome regions	450 K
Piston crown regions	450 K
Cylinder wall regions	400 K

The computational fluid dynamics (CFD) code, ES-ICE (expert solver for internal combustion engines) and STAR-CD (simulation of turbulent flow in arbitrary regions–computational dynamics) has been used to solve the discretized navier–stokes equations. The standard k–ε model with standard wall function has been employed for physical modeling. The program is based on the pressure-correction method and uses the PISO algorithm (Pressure Implicit Splitting of Operators). The first order upwind differencing (UD) scheme is used for the momentum, energy and turbulence equations and the temporal discretization is implicit. Spatial discretization is done using the upwind differencing scheme for momentum, turbulent kinetic energy/dissipation and temperature, and central differencing scheme for density. Temporal discretization is done using the Euler explicit scheme. ECFM-3Z combustion model is used to characterize ignition and combustion. The Reitz–Diwaker model[18] is used to characterize droplet break-up, with rebound

boundary condition at the walls. The model employed to determine the rate of change of size of droplets is that of Reitz and Diwakar[18], which mathematically represents instability of droplets by a critical value of the Weber number. Monotone Advection and Reconstruction Scheme (MARS)[24] is used to discretise species scalars. NOx emission is modelled by using extended Zeldovich mechanism. The soot emission model written in the Arrhenius single step form which considers the rate of change of soot mass is used to model soot emissions. The initial values of pressure and temperature are considered as homogeneous in the whole domain. The initial turbulent intensity is set at 10 % of the mean flow, and the integral length scale is set at 0.1 m. Temperatures at the cylinder head, the cylinder wall and the piston bowl that form the walls of the combustion chamber are specified as given in table 3.

Fuel injection is accomplished using lagrangian multiphase droplets. Vertex data is used for interpolation method and under-relaxation factor of lagrangian sources is set at 0.5. The droplet trajectory maximum file size is kept at 400 Mb, where maximum number of parcels are 500000. Turbulent dispersion, collision model and gravity effects for the droplets are taken into account. For droplet breakup, Reitz model is considered and to account for droplet wall interaction, Bai spray impingement model is accounted. Wall heat transfer, thermal break-up and boiling effects are also considered when the droplets encounters the hot environment. $C_{14}H_{30}$ (N-Tetradecane) is selected as fuel from the NIST table because it has the correct liquid fuel density. When this fuel evaporates, it will evaporate to $C_{12}H_{26}$. Huh atomization model is used. The injector nozzle L/D is chosen to be 6 and its coefficient of discharge is 0.7. Injection temperature is set at 310 K. The injector hole diameter is 0.4 mm and a separate input table for fuel mass flow rate is used to specify the injection timings and corresponding distribution of flue mass flow rates.

Results and Discussion

After generating the grid and applying the boundary and initial conditions, the time accurate computations are allowed until the residual reaches below the specified value.The time step chosen is 7.58 μs or 0.05°CA from 680°CA to 700°CA. Since the auto-ignition start after fuel injection, time step is decreased to 3.79 μs or 0.025°CA from 700°CA to 800°CA. The residual values for momentum (for all the three coordinates) and temperature are set as $1x10^{-3}$, and for pressure as $1x10^{-4}$ and turbulence kinetic energy and turbulence dissipation as $1x10^{-3}$. The monitor output frequency is set after every 5 timesteps and the backup frequency for writing all combustion and emission data in a file occurs after every 400 timesteps. Figure 2 shows the residual history of mass, momentum, enthalpy and turbulent kinetic energy. Figure 3 shows the spray in a mexican hat piston bowl at TDC. The motion of the dispersed phase will be influenced by that of the continuous one and vice versa via displacement and inter-phase momentum, mass and heat transfer effects. The strength of the interactions will depend on the droplet's size, density and number density. If the flow is laminar, each element released from a point will follow a smooth unique trajectory, i.e. the motion is deterministic. On the other hand, individual elements introduced into a turbulent carrier flow will each have their own, random path due to interaction with the fluctuating turbulent velocity field. Elements may also interact with each other (i.e. collision). If the dispersed phase is volatile, soluble or reactive, mass transfer occurs between the phases. This is accompanied by inter-phase heat transfer, which may also arise due to the inter-phase temperature differences. The size change may also be produced by fluid-dynamic forces acting on the dispersed elements, causing them to break up into smaller elements. Inter-element collision processes may also produce the opposite effect, i.e. size increase due to coalescence or agglomeration.

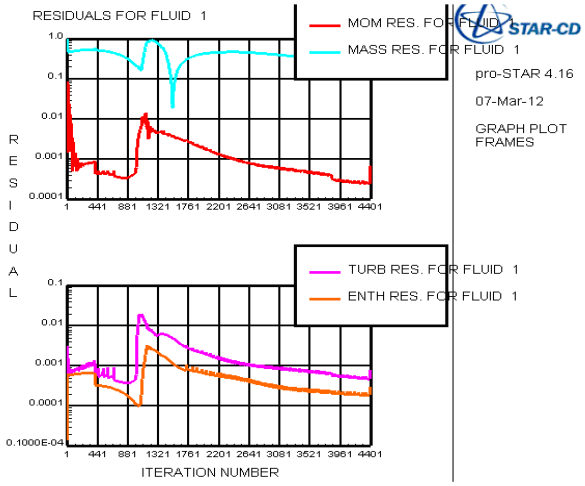

Figure-2
Residuals

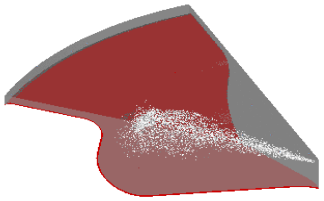

Figure-3
Fuel spray at TDC (720 deg CA)

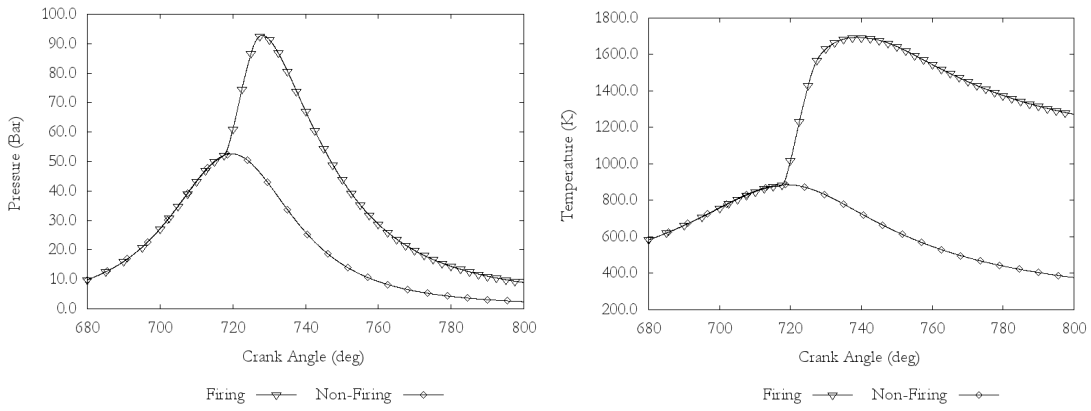

Figure-4
Cylinder averaged pressure and temperature

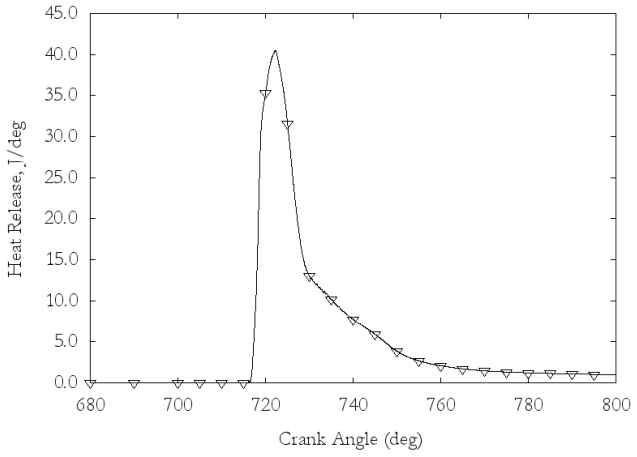

Figure-5
Cylinder Averaged heat release

For prediction of the auto-ignition delay, tabulated ignition data are used which are stored in look-up tables that are available in STAR-CD for different fuels. This table is generated based upon chemical kinetic calculations adopting complex reaction schemes. The tabulated values are stored as functions of the parameters such as pressure, temperature, fuel/air equivalence ratio and residual gas content. For the actual determination of the auto-ignition delay time in the CFD simulation, a transport equation for an auto-ignition indicator species is solved with the formation rate derived from the tabulated values. Once the local value of the indicator species attains a certain threshold value, auto-ignition is initiated. Fuel consumption is then controlled by a characteristic chemical time-scale which ensures rapid combustion after auto-ignition[15]. Figure 4 shows the pressure and temperature averaged data against crank angle (CA) for firing and motoring conditions. The motoring pressure is 50 bar at TDC and peak pressure is 92 bar at 7^{o} CA after TDC. The air fuel mixture inside the cylinder is overall lean and leads to slow burning rate and slowly raises the pressure and temperature inside the cylinder. Hence, with the availability of air for complete combustion and longer combustion duration, the fuel burns in diffusion mode with lower peak heat release rate and maximum cumulative heat release. The averaged heat release (figure 5) is obtained from the equation (14) of first law of thermodynamics assuming the absence of blow-by gases.

$$\frac{dQ}{d\theta} = \frac{1}{\gamma - 1} V \frac{dp}{d\theta} + \frac{\gamma}{\gamma - 1} P \frac{dV}{d\theta} \qquad (14)$$

Diesel particulates consist mainly of combustion generated carbonaceous material (soot) on which some organic compounds (arisen mainly from unburned fuel and lubricating oil) have been absorbed. Particulate material is distributed over a wide size range typically from 20 nm to 10 µm, which is often used as an estimation of soot. Other particulate matter constituents are: unburnt or partially burned fuel. Soot is formed from unburned fuel that nucleates from the vapor phase to a solid phase in fuel-rich regions at elevated temperatures. Hydrocarbons or other available molecules may condense on, or be absorbed by soot depending on the surrounding conditions. During steady-state engine operation, net soot production is mainly dependent on engine load. As the load increases, more fuel is injected into the cylinders, increasing the temperatures in the fuel-rich zones. Moreover, the duration of diffusion combustion is increased favoring soot formation, whereas the remaining time after combustion as well as the availability of oxygen, both of which enhance the soot oxidation process decreases; thus the production of soot is favored.

The hydrocarbon oxidation process during high temperature combustion is separated into three major reaction steps. First the fuel is partly oxidized to CO and to CO_2, followed by CO oxidation, and finally a post-flame equilibrium chemistry approach is applied which results in the final species

concentrations. Combustion reactions cover the relevant range of mixture composition from lean to rich and the different levels of residual gas content. NO can be formed in the reaction zone itself as well as in the post-flame region. The cylinder pressure rises during the combustion process and hence earlier burned gases are compressed to a higher temperature level. As a consequence of the high temperatures in the post-flame region and the simultaneously long residence times, the thermal NO formation in the burned gases usually exceeds the NO formed in the flame front and hence represents the main source of the nitric oxides. Figures 6 and 7 show the variation of cylinder averaged soot, CO, NOx and OH. All the quantities peak at TDC, whereas CO emissions are quite higher. After the breakup time, the liquid fuel of the spray packet disintegrates into many small drops. The Sauter mean diameter is the diameter of a representative drop, which has the same volume to surface area ratio. Since Sauter mean diameter is higher (figure 8) near TDC, there is more chance for fuel to be unburnt properly, hence resulting in higher emissions. Sensitive variations in droplet velocities are due to the swirl in the quiescent region in the cylinder at the end of compression stroke. Fig. 9 also indicates the presence of higher CO emissions from the contour details.

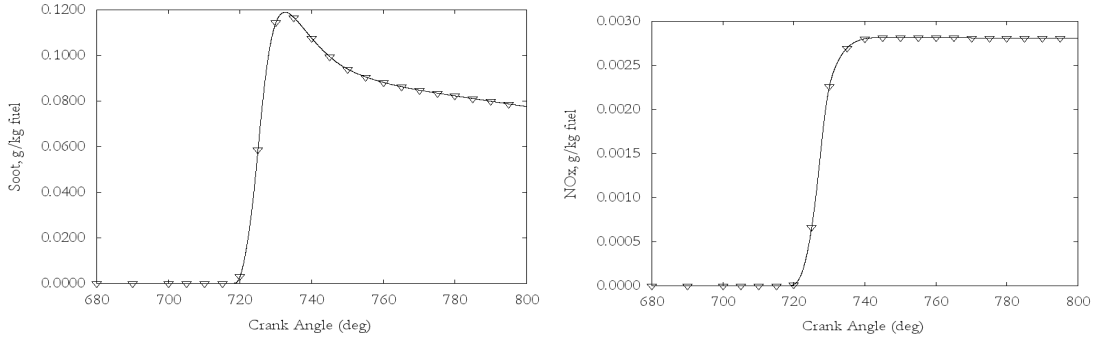

Figure-6
Averaged soot and NOx emissions

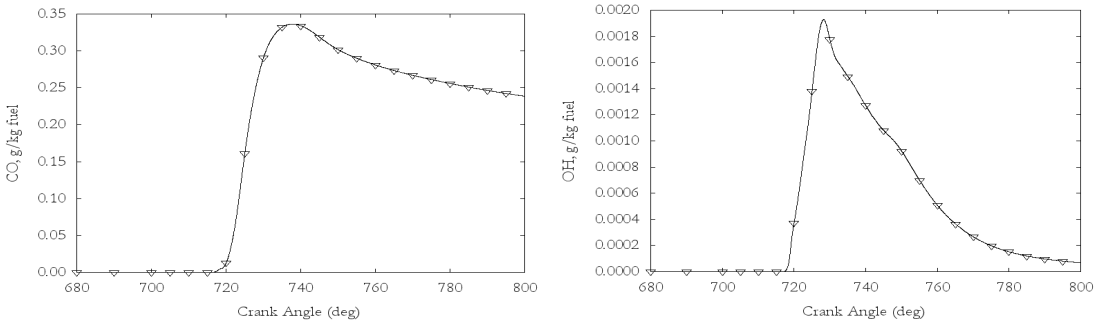

Figure-7
Averaged CO and OH emissions

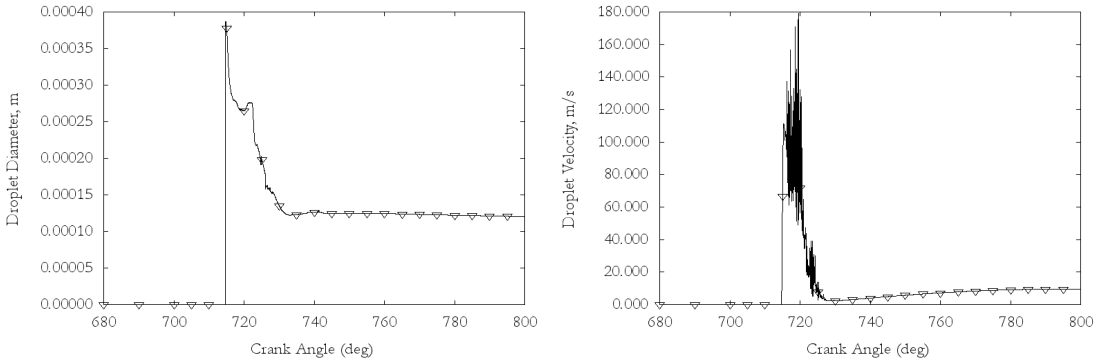

Figure-8
Mass averaged Sauter mean diameter and number averaged droplet velocity

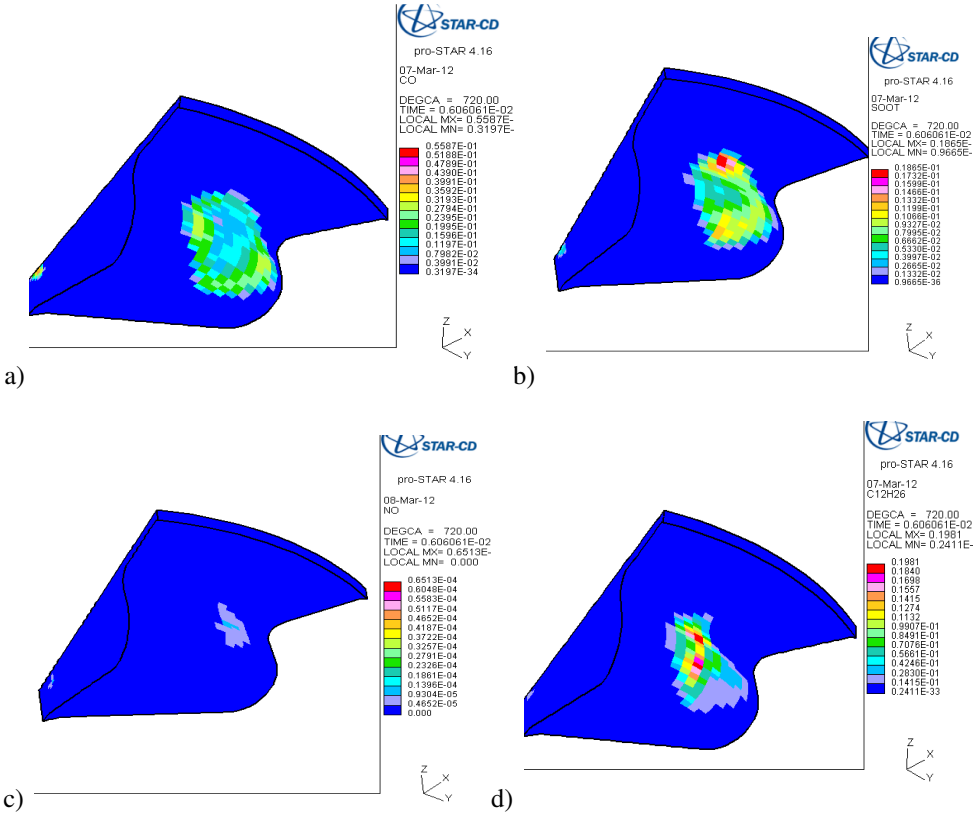

Figure-9
Contours at TDC of mass fractions of (a) CO, (b) Soot, (c) NO (d) $C_{12}H_{26}$

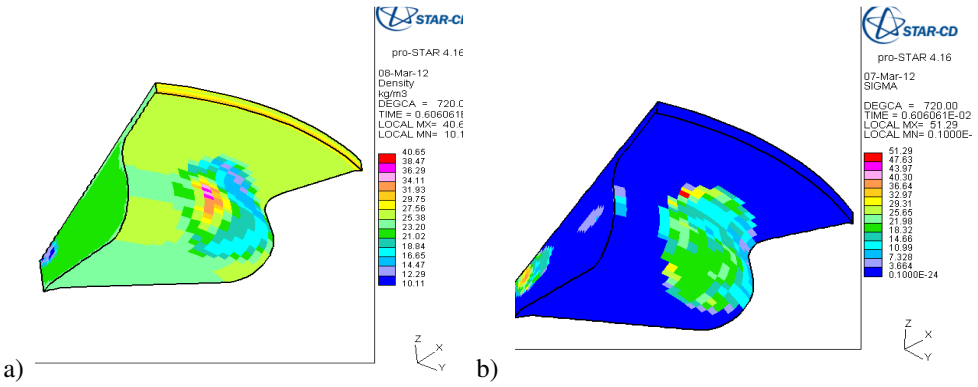

Figure-10
Contours at TDC of (a) Mixture density , (b) Flame surface density

The density of the reactant product mixture seems to be varying from 10 kg/m^3 in bowl region to 40 kg/m^3 near liquid film on the bowl wall (figure 10a). During the glow phase, fuel in the gas is burnt at the same rate as in the flame kernel particles. Once a kernel particle has burnt all its fuel, its excess energy is transferred to the gas and a flame surface density is initialized. Figure 10b shows the flame surface increases at the periphery of the fuel spread region in the piston bowl wall where the reaction starts. Hence the simulation of combustion and emission inside a DI engine gives clear picture in understanding the phenomenon of species formation and flame growth. Moreover, fruitful information on reacting species and combustion chemistry are clearly studied to enhance the performance and decrease the emissions.

Conclusion

Computational Fluid Dynamics (CFD) investigation is carried out to simulate the combustion and emission in the direct injection Diesel engine cylinder. Extended coherent flame

model, applicable in three zones is used in the simulation. Based on the overall performance and emission characteristics, the following conclusions are drawn from the present investigation: Peak pressure occurs at 7^{o}CA after TDC under firing conditions whereas at 0^{o}CA after TDC under non-firing conditions. Peak heat release occurs at TDC and peak temperature occurs at 20^{o}CA after TDC due to post flame emissions. Emissions increase at 0^{o}CA after TDC. The increasing trend is found to increase with the fuel injected in the cylinder. NOx emissions are higher at peak temperatures. Soot and CO emissions are higher at few degrees of CA after TDC.

The numerical modeling of the combustion and emissions give clear understanding in the heat release and formation of reactant species in the direct injection Diesel engine.

References

1. Stiesch G., Modeling engine spray and combustion processes, Springer Publications, 101-271 **(2003)**

2. Kimura S., Aoki O., Kitahara Y. and Aiyoshizawa E., Ultra-clean combustion technology combining a low-temperature and premixed combustion concept for meeting future emission standards, *SAE paper* 2001-01-0200 **(2001)**

3. Park S.W. and Reitz R.D., Numerical study on the low emission window of homogeneous charge compression ignition diesel combustion, *Combust Sci. Tech.* **179,** 2279–2307 **(2007)**

4. Lee S., Gonzalez M.A. and Reitz R.D., Effects of engine operating parameters on near stoichiometric diesel combustion characteristics, *SAE paper* 2007-01-0121 **(2007)**

5. Nevin R.M., Sun Y., Gonzalez M.A., Reitz R.D., PCCI investigation using variable intake valve closing in a heavy duty diesel engine, *SAE paper* 2007-01-0903 **(2007)**

6. Kimura S., Aoki O., Kitahara Y., Ogawa H., New combustion concept for ultraclean and high-efficiency small DI diesel engines, *SAE paper* 1999-01-3681 **(1999)**

7. Pathak S., Turbocharging and Oil Techniques in Light Motor Vehicles, , *Res. J. Recent Sci*., **1(1)**, 60-65 **(2012)**

8. Yenneti K.I. and Sharma R., CO2 Emission Reduction potential through improvements in technology from Civil Aviation Sector in India - A Case of Delhi-Mumbai Air Route, *Res. J. Recent Sci*.,**1(ISC-2011)**, 134-144 **(2012)**

9. Béard P., Colin O. and Miche M., Improved modeling of DI Diesel engines using sub-grid descriptions of spray and combustion, *SAE Paper* 2003-01-0008 **(2003)**

10. Warsi Z.V.A., Conservation form of the Navier-Stokes equations in general non-steady coordinates, *AIAA Journal*, **19**, 240-242 **(1981)**

11. Jones W.P., Prediction methods for turbulent flames, Hemisphere, Washington, D.C., 1-45, **(1980)**

12. Launder B.E., Spalding, D.B., The numerical computation of turbulent flows, *Comp. Meth. in Appl. Mech. and Eng*., **3**, 269-289 **(1974)**

13. El Tahry S.H., k-ε equation for compressible reciprocating engine flows, *AIAA J. Energy*, **7(4)**, 345-353 **(1983)**

14. Pope S.B., Turbulent Flows Part II. Modeling and Simulation, Paperback edition, Cambridge University Press, 373-382 **(2000)**

15. Colin O. and Benkenida A., The 3-Zone Extended Coherent Flame Model (ECFM3Z) for computing premixed/diffusion combustion, *Oil & Gas Science and Technology – Rev.* IFP, **59(6)**, 593-609 **(2004)**

16. Metghalchi M. and Keck J.C., Burning velocities of mixtures of air with methanol, isooctane, and indolene at high pressure and temperature, *Combust. Flame*, **48**, 191-210 **(1982)**

17. Nicholls J.A., Stream and droplet breakup by shock waves, *NASA SP–194*, 126–128 **(1972)**

18. Reitz R.D., Diwakar R., Effect of drop breakup on fuel sprays, *SAE Technical Paper Series,* 860469 **(1986)**

19. Bai C., Gosman A.D., Development of methodology for spray impingement simulation, *SAE Technical Paper Series* 950283 **(1995)**

20. Pershing D.W. and Wendt J.O.L., Pulverised coal combustion: the influence of flame temperature and coal composition on thermal and fuel NOx, 16th Symp. (Int.) on Combustion, *The Combustion Institute*, 389-399 **(1977)**

21. De Soete G.G., Heterogeneous N_2O and NO formation from bound nitrogen atoms during coal char combustion, 23rd Symp. (Int.) on Combustion, *The Combustion Institute*, 1257-1264 **(1990)**

22. Millares C.A.R., Mathematical Modeling of Fuel NO Emissions from pf Burners. PhD Thesis, Imperial College of Science, Technology and Medicine, University of London **(1992)**

23. Karlsson A., Magnusson I., Balthasar M. and Mauss F. Simulation of soot formation under Diesel engine conditions using a detailed kinetic soot model, *Proc. SAE Int. Congr. and Expo*., Detroit, Michigan, USA, 23-26 February, SAE Technical Paper Series 981022 **(1998)**

24. Star-CD user guide, version 4.16.001, CD-adapco **(2011)**